Journal of Hydrology 389 (2010) 276–288

Contents lists available at ScienceDirect

Journal of Hydrology

journal homepage: www.elsevier.com/locate/jhydrol

Spatial and temporal variations in streambed hydraulic conductivity quantified with time-series thermal methods

Christine E. Hatch [a,*,1], Andrew T. Fisher [a,b], Chris R. Ruehl [a,2], Greg Stemler [a,3]

[a] Earth and Planetary Sciences Department, University of California, Santa Cruz, E&MS A232, 1156 High Street, Santa Cruz, CA 95064, USA
[b] Institute for Geophysics and Planetary Physics, University of California, 1156 High Street, Santa Cruz, CA 95064, USA

ARTICLE INFO

Article history:
Received 27 October 2009
Received in revised form 16 March 2010
Accepted 28 May 2010

This manuscript was handled by Philippe Baveye, Editor-in-Chief, with the assistance of C. Corradini, Associate Editor

Keywords:
Hydraulic conductivity
Streambed seepage
Heat as a tracer
Surface water–ground water interaction
Pajaro River

SUMMARY

We gauged and instrumented an 11.42-km long experimental reach of the Pajaro River, central coastal California, to determine rates of streambed seepage (loss and hyporheic exchange) using reach averaged and point specific methods. We used these data to assess changes in streambed hydraulic conductivity with time, as a function of channel discharge and associated changes in sediment scour and deposition. Discharge loss along the experimental reach was generally 0.1–0.3 $m^3 s^{-1}$ when channel discharge was $\leqslant 2 m^3 s^{-1}$, with most of the loss occurring along the lower part of the experimental reach. Point specific seepage rates, determined using time-series analysis of streambed thermal records, indicate seepage rates as great as $-1.4 m day^{-1}$ (downward into the streambed). Seepage rates varied spatially and with time, with greater seepage occurring along the lower part of the reach and during the summer and fall. Seepage rate and hydraulic gradient data show that streambed hydraulic conductivity was 10^{-6}–$10^{-4} m s^{-1}$ along the experimental reach, with lower conductivity determined later in the dry season, as sediment was deposited on the streambed during low flow conditions. These results suggest that models of surface water–ground water interactions may benefit from inclusion of relations between stream discharge, sediment load, and streambed hydraulic properties.

1. Introduction

1.1. Motivation and goals

Streams and aquifers interact over a range of temporal and spatial scales. A significant fraction of ground water recharge occurs through streambeds, and aquifers can provide the primary input to streams during the dry season as baseflow (Allen et al., 2004; Sanford, 2002; Whiting, 2002). Water also moves back and forth between the surface and subsurface during hyporheic exchange, a process that influences the quantity and quality of channel discharge, riparian conditions, and the magnitude and timing of nutrient export (Bencala, 1993; Fanelli and Lautz, 2008; Puckett et al., 2008; Smith et al., 2008). These and other processes occur heterogeneously and dynamically within stream–aquifer systems, responding to changes in channel geometry, sediment load, streambed lithology, and water table elevation. Additional complexity is associated with stream diversions, ground water pumping, and other human activities, and by changing regional climate and hydrology (Goderniaux et al., 2009; Groves et al., 2008; Jefferson et al., 2008; Loheide et al., 2009; Taniguchi et al., 2008). Understanding and responding to changes to surface water–ground water interactions requires developing a process-based understanding of how these systems function.

Considerable effort has been applied in recent years to develop tools that can be used to quantify the locations and timing of flow between streams and aquifers, and to use field observations to design and constrain computer simulations (Becker et al., 2004; Kalbus et al., 2006; Rosenberry and LaBaugh, 2008). One class of field measurements is applied at a reach-scale. Differential gauging is useful for determining the net change in discharge, but provides little information on the movement of water back and forth between the channel and nearby subsurface at a scale that is shorter than the length of the reach over which measurements are made. Tracer discharge studies are similarly useful for quantifying effective channel and exchange metrics, and can be helpful for assessing the net gain of unlabeled water along a reach (Haggerty et al., 2008; Runkel, 1998,

* Corresponding author. Tel./fax: +1 775 784 4509.
E-mail addresses: christine_hatch@gmail.com, chatch@unr.edu (C.E. Hatch), afisher@ucsc.edu (A.T. Fisher), Greg.Stemler@amec.com (G. Stemler).
[1] Present address: Department of Geological Sciences and Engineering, University of Nevada, Reno, NV 89557, USA.
[2] Present address: Department of Civil and Environmental Engineering, University of California, Davis, One Shields Avenue, 2001 Engineering III, Davis, CA 95616, USA.
[3] Present address: AMEC Geomatrix, Inc., 2101 Webster St # 12, Oakland, CA 94612, USA.

0022-1694/$ - see front matter © 2010 Elsevier B.V. All rights reserved.
doi:10.1016/j.jhydrol.2010.05.046

2000; Wondzell et al., 2009). Other field measurements are applied at a point scale. Seepage meters are used to quantify the rate of fluid entering or leaving a channel across a small area of streambed, typically during deployments lasting no more than a few days (Lee and Cherry, 1978; Murdoch and Kelly, 2003; Rosenberry, 2008). Streambed piezometers are used to measure head differences between the channel and the shallow subsurface. When combined with independent estimates of streambed hydraulic conductivity, piezometer data can be used to estimate flows to and from the channel (Barlow and Coupe, 2009; Fanelli and Lautz, 2008; Schmidt et al., 2007).

Field measurements are often used to constrain numerical models that include surface water–ground water interactions based on the concept of riverbed conductance (e.g., MODFLOW (McDonald and Harbaugh, 1988), VS2DI (Healy, 2008; Healy and Ronan, 1996), HST3D (Kipp, 1987, 1997), TOUGH2 (Pruess, 1994; Pruess et al., 1998), and HydroGeoSphere (Therrien et al., 2006)). We use the nomenclature for streambed conductance introduced with the popular, public-domain code MODFLOW to illustrate how dynamic riverbed hydraulic conductivity can influence surface water–ground water interactions represented with a numerical model. Nomenclature differs with other models, but the concept is similar.

Riverbed conductance (*CRIV*) was represented in the initial release of MODFLOW (McDonald and Harbaugh, 1988) based on pragmatic assumptions concerning interactions between surface water and ground water, with *CRIV* to/from a model cell defined as:

$$CRIV = \frac{KLW}{M}$$

where K = hydraulic conductivity of the riverbed, L = reach length, W = reach width, and M = thickness of the riverbed. One or more rules are applied to determine the flow of water between the river and aquifer during every model time step, using river conductance as a coefficient of proportionality that relates flow to head gradient.

Different riverbed conductance values can be applied to different parts of a model grid, representing variations in lithology, geometry, and/or the thickness of the riverbed, and some models allow for conductance to vary with river stage, often considered to result from changes to the wetted perimeter as the river water surface rises and falls (e.g., Prudic et al., 2004). However, numerical models have generally not included temporal variations in the hydraulic conductivity of a riverbed at fixed locations, in part because there has been a lack of quantitative data upon which to base the assignment of dynamic streambed conductivity. Changes in discharge velocity influence stream capacity and flow competence (the largest particle a stream can transport), and this causes sediment to be added or removed from the streambed, simultaneously changing the hydraulic properties of the streambed and the channel geometry. There are also variations in sediment inputs to a stream channel at different times of the year, and at different times during a single storm event, and there may be hysteretic relations between stage, discharge, and sediment load. For these reasons, it is challenging for a surface water–ground water model to represent the spectrum of processes necessary to link quantitative dependencies between streamflow, stage, sediment transport, and streambed properties.

We present field data that quantify changes to streambed properties along an experimental reach. Data include reach-scale and point-scale measurements and determinations of net and local stream discharge losses, allowing a daily assessment of streambed seepage and hydraulic conductivity. Results of this study illustrate that there can be significant (order of magnitude) temporal changes to properties that impact surface water–ground water interactions, and suggest that it may be beneficial to take these properties and dynamics into account in modeling streambed seepage in such systems.

2. Field and experimental setting

2.1. The Pajaro River and Pajaro Valley ground-water basin

The Pajaro River is a fourth-order stream draining a 3400 km^2 basin in central coastal California, USA, and emptying into Monterey Bay (Dupré et al., 1980; Hanson, 2003; Johnson et al., 1988) (Fig. 1). The watershed is bounded laterally by coastal mountains and underlain by Cretaceous granodiorite basement. Principal water-bearing units in the Pajaro Valley ground-water basin are sedimentary rocks composed of cyclic packages of eolian, marine and fluvial sediments that form three principal, laterally extensive aquifer units that are discontinuously separated by finer grained layers. The aquifer units are (from shallowest to deepest): quaternary alluvium (upper and lower), Pleistocene Aromas Formation (mainly eolian and fluvial sand/gravel deposits), and the Pliocene Purisima Formation (fluvial sand and gravel, marine shale, silt, sand and clay) (Hanson, 2003) (Fig. 1C). In the Pajaro Valley ground-water basin, these aquifer deposits have a maximum thickness of 1200 m (Muir, 1972).

Mean annual precipitation in the Pajaro River watershed is 50 cm yr^{-1} (CARA, 1997). Mean daily temperatures are 3–23 °C, and 90% of annual precipitation typically falls between October and May. Hydrologic conditions in this area vary on an annual cycle referred to as the "water year," which begins on 1 October (of the previous calendar year, water day 1) and ends on 30 September (water day 365). Recharge to the Pajaro Valley ground-water basin occurs through deep percolation during the rainy season, and through streambed seepage and irrigation returns throughout much of the year. The climate and well-drained soils enable year-round agriculture in the Pajaro Valley, the vast majority of which is supported by irrigation supplied by ground water. There has been a steady increase in demand for fresh water in the Pajaro Valley to meet agricultural and municipal needs in recent decades, and this has lead to overdraft of limited ground water supplies (PVWMA, 1999, 2001). The current rate of ground water extraction in the basin from the Alluvial and underlying Aromas aquifers is $\sim 8.5 \times 10^7$ m^3 yr^{-1}, considerably more than the estimated sustainable basin yield given recent patterns of pumping (PVWMA, 2001). Long-term overdraft has resulted in seawater intrusion near the coast and lowering of water levels in wells throughout the basin, with an estimated annual loss of $\sim 1.1 \times 10^7$ m^3 of freshwater storage (PVWMA, 2001). As in many ground-water basins, there are large uncertainties in the magnitude of ground water overdraft, especially because of limited metering (not required statewide in California) and because of uncertainties of the locations, timing, and magnitude of ground water recharge. Anticipated continuing population growth, agricultural and municipal demand, and regional changes to hydrologic conditions are likely to complicate future fresh water resource management in the Pajaro Valley ground-water basin (Bower et al., 2004; Hanson and Dettinger, 2005; Jefferson et al., 2008; Lettenmaier et al., 1999; Snyder et al., 2002; Taniguchi et al., 2008).

Municipal, agricultural, and gravel-mining activities have resulted in degradation of surface water quality in Pajaro River, culminating in its 1998 designation as impaired by various contaminants including sediment (or siltation) under the Clean Water Act section 303(d) by the US Environmental Protection Agency (California, 2005; EPA, 2009; Rose and Adams, 2009). Excessive sediment and contaminants in streams affect surface and ground water quality. As shown in this study, impairment by sediment load also has implications for the nature of surface water–ground water interactions in the basin.

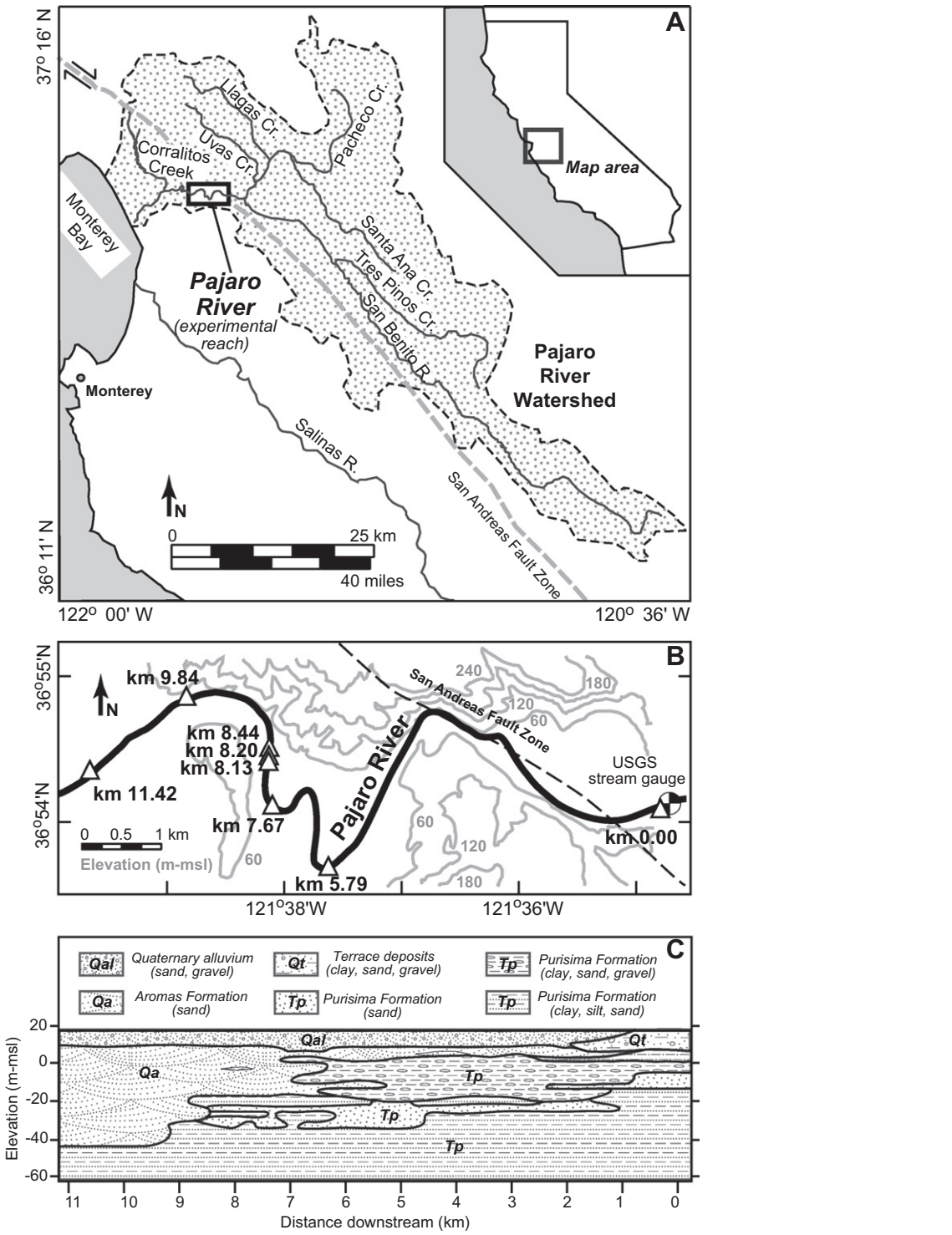

Fig. 1. Study setting. (A) Map of the Pajaro River watershed, central coastal California, USA. Inset shows location of experimental reach. (B) Pajaro River experimental reach. Piezometer locations are marked in distances (km) downstream from the USGS stream gauging station (11159000, Pajaro River at Chittenden, CA), km 0.00. (C) Simplified geologic cross section along the Pajaro River experimental reach expanded from compilation of well logs adjacent to river (adapted from Stemler, 2005).

2.2. Pajaro River experimental reach

An experimental reach was established on the Pajaro River as part of a multi-year research project to assess the magnitude of stream seepage losses, quantify the nature of hyporheic exchange, and evaluate the influence of both processes on nutrient cycling, load, and export (Ruehl et al., 2007, 2006). The experimental reach begins at a US Geological Survey (USGS) stream gauging station (11159000, Pajaro River at Chittenden, CA) and ends 11.42 km downstream (Fig. 1B). This reach of the Pajaro River was chosen specifically because it had no known inflows or diversions during the period of study, allowing for a detailed and precise determination of water mass balance, and because anecdotal information suggested that the reach lost measurable discharge under relatively low flow conditions. Mean daily discharge entering the top of the experimental reach is 5 $m^3 s^{-1}$, the highest discharges (35–

200 $m^3 s^{-1}$) typically occur between January and March, and the lowest discharges (<0.3 $m^3 s^{-1}$) typically occur between July and October, coinciding with the wettest and driest parts of the year, respectively. Most field experiments and direct measurements of discharge in the present study were conducted during the second half of the water year, when there was no precipitation or flow into the channel from adjacent hillslopes, and streamflow was relatively stable. Stream width averaged 5–15 m, depths ranged from 0.1 to 1.0 m, and stream velocities ranged from 0.1 to 0.6 m s^{-1} along the experimental reach during this study.

Observation, measurement, and sampling points were established along the experimental reach and named according to river distances downstream from the USGS gauging station at the top of the reach. The Pajaro River flows through a steep-walled valley along the first 4 km of the experimental reach, and is underlain by relatively thin layers of terrace deposits and the Purisima Formation (essentially a bedrock channel). The valley widens considerably along the rest of the experimental reach, where the river is underlain by thick alluvial deposits and the Aromas formation, the primary aquifer for the Pajaro Valley (Fig. 1). The stream gradient over the entire reach is 0.1%, with greater typical stream velocities in the upstream part of the reach and lower velocities as the Pajaro Valley widens downstream.

3. Methods

3.1. Stream gauging

We measured stream discharge repeatedly at multiple sites along the experimental reach using the velocity–area method (Fig. 1B) (Buchanan and Somers, 1969; Rantz, 1982) with a pygmy Price flow meter. Discharge profiles were collected in carefully selected locations where the channel geometry was favorable for measurement, and monitored carefully so that no more than 5% of discharge was represented by any single measurement within a cross-channel profile. Under good to excellent measurement conditions, which existed when data was collected for this study, errors associated with these measurements are generally thought to be 5–10% (Metzger, 2002; Sauer and Meyer, 1992).

Stream stage was measured using a fixed staff plate at km 0.0 and at km 11.42, and rating curves were developed and maintained for each site relating discharge and stage. Rating curves were revised regularly as needed because of changes to channel geometry. Stage values were acquired at 15-min intervals at km 0.00 and km 11.42 using pressure measurements. Instruments at km 0.00 were maintained by the USGS (station 11159000), whereas instruments at km 11.42 were installed and maintained by UCSC researchers. The UCSC pressure gauge was field calibrated during installation and checked periodically to correct for drift relative to staff plate readings.

Differential discharge gauging was used to quantify net losses or gains along sections of the experimental reach. Periodic seepage runs (two or more discharge measurements along the reach on the same day) were used to quantify the locations, timing, and magnitude of seepage losses or gains along the reach. High-resolution stream stage data were used to generate discharge values at 15-min intervals, and these were averaged to generate mean daily discharge values at each gauge location. The total channel loss from the top to the bottom of the experimental reach was calculated as $\Delta Q = Q_{0.00} - Q_{11.42}$, and the percent lost by each observation point was calculated as $\Delta Q_{obs\ km}\ (\%) = (Q_{0.00} - Q_{obs\ km})/\Delta Q) \times 100$.

During this study, stream discharge was measured at flows no greater than 4 $m^3 s^{-1}$. Conditions in the channel were too dangerous for wading at higher flows. Also, measurements and sampling were focused on conditions after the end of the rainy season, when there was no hillslope runoff or other input into the experimental reach, simplifying water balance calculations.

3.2. Streambed piezometers and hydraulic gradient measurements

Streambed piezometers were constructed from 3.2 cm (1-¼ in) schedule-40 PVC pipe, steel drive-points, and 0.1 m screened intervals. Piezometers were driven into the streambed with a slide hammer and drive rod at nine locations along the experimental reach (Fig. 1B), in cross-sections at six sites and as individual installations at three sites. Piezometers penetrated 1–2 m below the base of the stream, with screened intervals placed 0.72–1.63 m below the streambed. This installation method minimized disturbance to the sediment surrounding the piezometer, and avoided the introduction of sediment into the water column. Hydraulic gradient measurements were made by hand periodically throughout the study period using the piezometers. Piezometer caps were removed and a riser pipe was attached if needed, then the water level in the riser was allowed to equilibrate prior to measuring the head difference between the stream and the streambed. Piezometers that were damaged or removed by high storm discharges throughout the study were replaced when possible, and sedimentation and scour was assessed during periodic site visits.

3.3. Streambed thermal data collection and analysis methods

Thermal piezometers were instrumented with 2–4 autonomous, temperature measuring and logging instruments, set to record fluid temperature at 15-min intervals throughout water years 2003–2006. Hooks were placed inside the top caps, and 3-mm diameter nylon accessory cord was used to suspend the temperature loggers in fixed positions (Fig. 2). Temperature resolution and accuracy were 0.02 °C and 0.2 °C, respectively (Onset HOBO Water Temp Pro), or 0.2 and 0.4 °C (Onset Stowaway Tidbit) over the measurement range used in this study. Resolution and accuracy were quantified prior to instrument deployment using an extremely stable, stirred-water Hart Scientific calibration bath monitored with a reference sensor having resolution and accuracy of 0.002–0.003 °C. Temperature instrument arrays were deployed

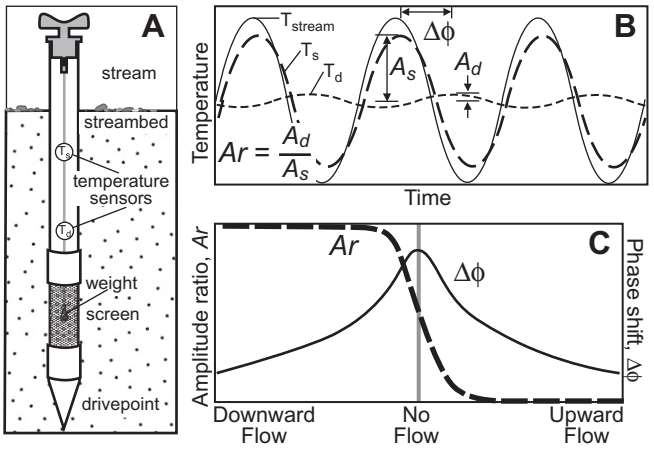

Fig. 2. Diagrams illustrating acquisition of streambed temperature records and time-series analytical method (Hatch et al., 2006). (A) Streambed piezometer with temperature sensors. Shallow (T_s) and deep (T_d) sensors are shown, but typical installations used in the present study comprise two to four thermal instruments at different depths below the top of the streambed. (B) Schematic temperature versus time records from the stream (T_{stream}), a shallow (T_s) and a deep (T_d) sensor illustrating reduction in amplitude, amplitude ratio [$Ar = A_d/A_s$; ratio of deep (A_d) to shallow (A_s)] and shift in phase ($\Delta\phi$) with greater depth. (C) Schematic type curves illustrating the relationship between amplitude ratio (Ar), phase shift ($\Delta\phi$), and seepage rate and direction.

at low water levels or under dry conditions, then left for months at a time to record data. Instruments were recovered periodically when water levels were low enough to allow wading into the river, data were downloaded, and loggers were redeployed.

Thermal data were processed and interpreted to determine local rates of streambed seepage using a time-series approach (Hatch et al., 2006). Individual temperature records were band-pass filtered to isolate diurnal frequencies of temperature variations. Despite seasonal temperature variations in the stream of ~15 °C, daily amplitudes of 0.5–3 °C in the upper 1 m below the streambed were common throughout the water year. Pairs of filtered sensor records were analyzed to quantify the reduction in amplitude (and the amplitude ratio between deeper and shallower records) and the shift in phase once per day. These values were used to determine the local seepage rate based on the analytical solution to a one-dimensional, transient, conduction–advection–dispersion equation (equations shown by Goto et al., 2005; Hatch et al., 2006; Stallman, 1965).

Streambed seepage rates were calculated using thermal data based on these properties for saturated sandy streambed: porosity, $n = 0.375$, fluid and sediment densities of $\rho_f = 997$ kg m^3 and $\rho_s = 2650$ kg m^3, respectively, heat capacities of the fluid $c_f = 4180$ J kg^{-1} °C^{-1} and sediment $c_s = 800$ J kg^{-1} °C^{-1}, and thermal dispersivity of $\beta \sim 10^{-3}$ m. The baseline thermal conductivity, appropriate for a purely-conductive system in the absence of thermal dispersion, was set to $\lambda_0 = 1.58$ W m^{-1} °C^{-1} (the geometric mean of grain conductivity, $\lambda_g = 2.8$ W m^{-1} °C^{-1}, and fluid conductivity, $\lambda_f = 0.6$ W m^{-1} °C^{-1}). Sensor pairs used for seepage estimates were selected on the basis of having sufficient amplitude for analysis over the period of record and remaining saturated for as long as possible. Sensors pairs worked well when positioned at 10 cm and 45 cm below the streambed, or at 25 cm and 45 cm, with relative spacings of $\Delta z = 35$ cm or $\Delta z = 20$ cm, respectively.

This analysis method offers many advantages relative to forward modeling of thermal records, including speed and ease of data handling, and insensitivity to streambed sedimentation or scour (being based on sensor spacing rather than absolute depth), which was especially important in the present study. Seepage rates determined using the time-series thermal method applied in this study comprise the vertical component of the complete flow vector, accurate to the larger of 5–10% of the seepage rate or ±0.05 m day^{-1} (Hatch et al., 2006). There is a time lag associated with heat transport through PVC casing, but errors introduced by this lag are generally ⩽1% of the true flux (Cardenas, 2010). The method applied herein is robust for reasonable variations in physical parameters, but does not account for non-vertical flow conditions (e.g., Lautz, 2010).

3.4. Streambed hydraulic conductivity

We combined flow rate and head gradient values to calculate streambed hydraulic conductivity, K, using Darcy's law: $K = -q \cdot (dh\ dz^{-1})^{-1}$. K calculations were limited by the following conditions (to avoid the compounding influence of experimental error): (1) seepage magnitude is greater than 0.05 m day^{-1}, (2) the magnitude of the hydraulic gradient is greater than 0.01, and (3) gradient and seepage directions agree. In general, condition (3) was found to be untrue mainly when conditions (1) and/or (2) were violated (very small apparent flow rates and/or head gradients). In addition, data were only used from sensors that remained below the streambed for the duration of the thermograph (and were not exposed directly to the water column via scour). Gradient estimates were linearly interpolated between hand measurements, because instrumentation was not available to record pressure in piezometers continuously. Errors could be introduced if there were abrupt changes in the magnitude or sign of gradients, but gradient values were found to change gradually throughout the study period. The application of Darcy's law presumes steady state conditions for each calculation of a mean daily value, but this assumption is reasonable considering the high hydraulic conductivities of streambed materials (mainly sand and gravel) and the typical persistence of flow and seepage conditions. In addition, Darcy's law will provide an estimate of the harmonic mean of the vertical hydraulic conductivity over the applicable depth (dz), and the resulting value will be limited by the least conductive layer. The variations in hydraulic conductivity reported herein do not take into account actual changes in the thickness of the streambed, but are apparent or effective values for the complete interval between the base of the stream and the piezometer screen, as would be appropriate for use in regional (numerical) studies of surface water–ground water interactions.

4. Results

4.1. Discharge gauging and channel geometry

Thirty-two stream discharge campaigns (seepage runs) were completed over the duration of the study (2003–2006), with discharge measured at two or more locations along the experimental reach (Fig. 3). Discharge generally decreases downstream along the reach, with most of this loss occurring downstream of km 5.79 (Fig. 3), where clay and silt-rich lithologies become less common and coarser sediments are exposed along the streambed (Fig. 1C). Earlier studies demonstrated that evaporative losses along the experimental reach are ⩽10% of observed discharge losses (Ruehl et al., 2006), and data shown in the present study are restricted to times when there were no additional sources or sinks for water along the reach, so this loss comprises stream seepage almost exclusively. The measured loss of discharge in the reach was generally $\Delta Q \sim 0.1$–0.3 m^3 s^{-1}. On average, 16% of stream discharge losses occur along the upper 5.79 km of the reach, whereas the rest of the reach loses ~15% of the total loss per river kilometer. The lower part of the reach loses an average of 0.23 ± 0.1 m^3 s^{-1}, representing 30 ± 13% of total stream discharge when $Q \leqslant 2$ m^3 s^{-1}. The channel downstream from km 9.0 often became dry by late summer and remained dry until after the first significant precipitation of the subsequent water year. This corresponds to the section of streambed underlain by the thickest uninterrupted aquifer materials, and the increasingly thick and continuous Aromas formation, the primary basin aquifer.

Each stream discharge measurement generated a cross-channel profile of stream geometry, allowing us to track changes during the water year and from year to year. The geometry of the stream channel changed markedly during the measurement period, especially towards the lower end of the experimental reach (Fig. 4). The channel was often at its widest and deepest towards the end of the rainy season, and then became progressively smaller as flows decreased, along with the competence and capacity of the discharge. During 2004 the active part of the channel remained in essentially the same location, whereas the active channel migrated towards the left bank (looking upstream) during 2005 (Fig. 4B). The deepest part of the channel generally accumulated 0.1–0.3 m of sediment between the last storm of the year (water day ~200–220) and the end of the water year.

4.2. Apparent seepage rates and gradients from streambed piezometers

Seepage rates were determined with thermal sensors at multiple locations and time intervals during water years 2003–2006, but the most complete records were collected during 2004 and 2005; selections of data from these water years are shown to illustrate

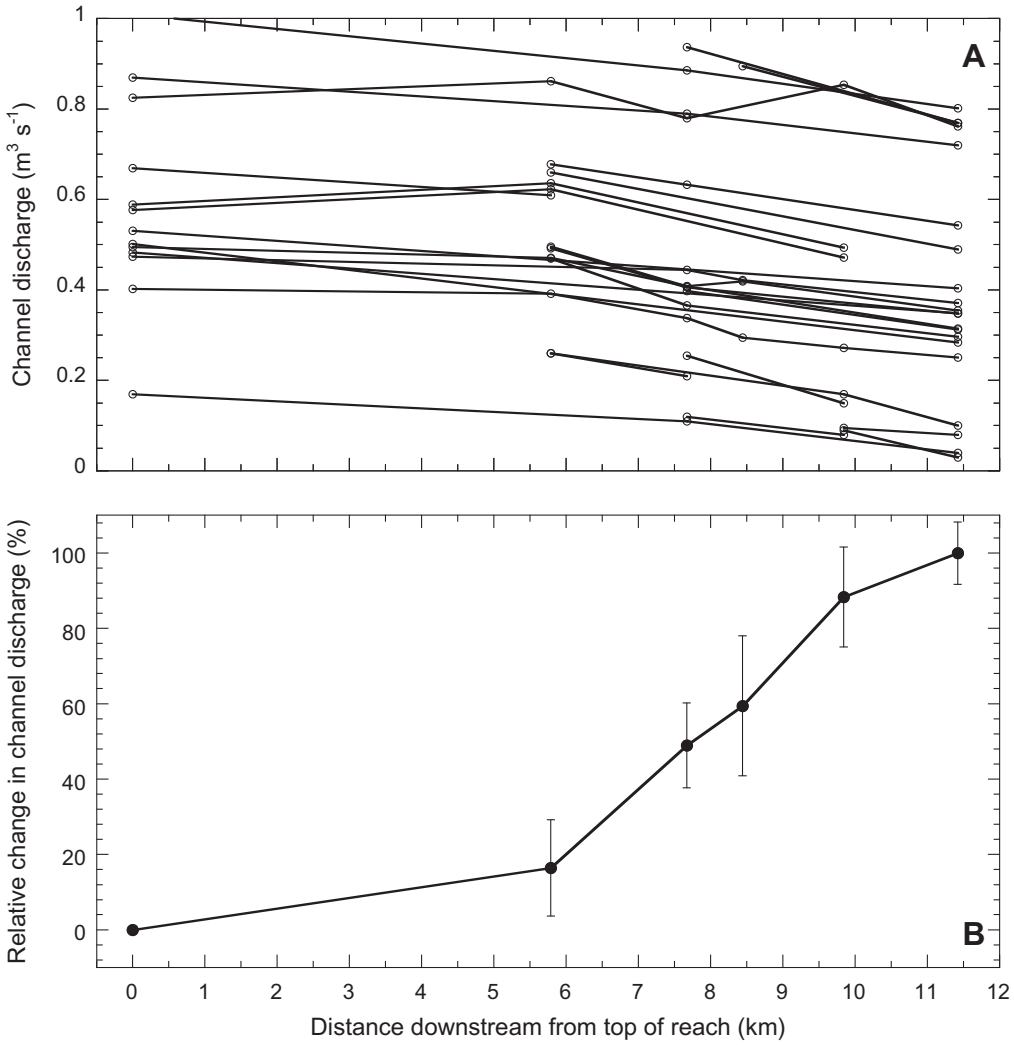

Fig. 3. Summary of 32 seepage runs on Pajaro River from 2003 through 2006 along the experimental reach. (A) Individual seepage runs: discharge ($m^3\ s^{-1}$) versus distance downstream (km). (B) Percentage loss of channel discharge. Error bars indicate standard deviation of measurements.

several characteristics of streambed seepage and properties. Thermal data used to estimate seepage rates shown here were collected along the entire experimental reach in streambed piezometers screened from 1.17 to 1.63 m below the base of the stream: two single piezometers along the upper part of the reach were deployed at km 0.00 and km 5.79, and piezometer profiles were deployed along the lower part of the reach, with two at km 8.13, four at km 8.44, and three each at km 9.84 and km 11.42 (Fig. 1B).

Seepage varied spatially and temporally throughout water years 2004 and 2005 (Figs. 5 and 6). During the second half of the water year, when the net loss of discharge from the experimental reach was 0.1–0.3 $m^3\ s^{-1}$, downward seepage generally increased with distance downstream (Fig. 5, Tables 1 and 2). One exception to this trend was apparent within a small-scale pool-riffle sequence between km 8.20 (bottom of pool and beginning of higher gradient stretch) and km 8.44 (bottom of riffle), from which thermal data indicated gaining conditions for much of water year 2005 (Fig. 5C). In the upper half of the experimental reach (km 0.00 and km 5.79), the thermal sensors indicate slow upward seepage or no seepage earlier in the water year, but downward seepage begins at water days 338 (water year 2004) and 296 (water year 2005), eventually reaching −0.3 m day^{-1}. There was downward seepage from the lower part of the reach (except within the pool-riffle sequence noted above) at −0.2 to −0.5 m day^{-1} at km 8.13, −0.3 to −1.3 m day^{-1} at km 9.84, and −0.3 to −0.7 m day^{-1} at km 11.42. Downward seepage at these sites generally remained steady or decreased slightly with time.

Hydraulic gradients varied from moderately positive to strongly negative along the experimental reach, and were greatest in magnitude near the bottom of the reach at km 9.84 and km 11.42 (Fig. 5D). The gradient at km 11.42 exceeded −1.0 towards the end of the water year, consistent with development of a vadose zone below the streambed (and below the depth of the piezometer screen), when the rate of seepage could not keep up with the rate of drainage from underlying sediment (e.g., Brunner et al., 2009a,b). The gradient at km 8.44 was positive in all four piezometers in water year 2005, consistent with seepage up and out of the streambed.

4.3. Spatial and temporal variations in streambed hydraulic conductivity

Calculated values of *K* indicate consistent spatial and temporal trends (Fig. 5E, Tables 1 and 2). *K* values are shown as a time series of calculations, based on daily seepage rates, interpolated head gradients, and application of Darcy's law. *K* was calculated in water year 2005 at km 0.00 only for the last part of the record, when the seepage rate was sufficiently rapid. Records at km 8.13, km

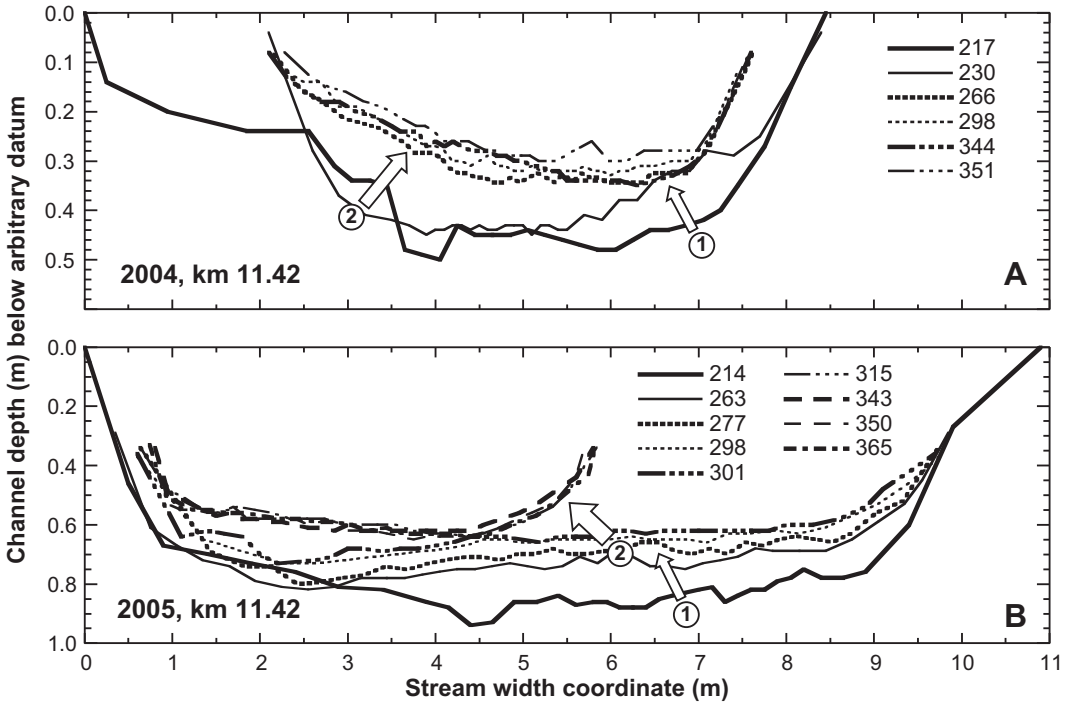

Fig. 4. Stream cross-sections of Pajaro River at km 11.42 collected during individual streamflow measurements between May and September on water days indicated (A) in water year 2004 and (B) 2005 illustrate the mobility of the bed sediments and morphologic changes to the streambed at these sites. Arrows indicate the order and evolution of bed shape, and areas of local aggradation and scour (~2× vertical exaggeration).

8.44, km 9.84, and km 11.42 allowed generation of longer time series of K values. Mean streambed K at km 8.13, km 9.84, and km 11.42 was 10^{-4} m s^{-1}, 5×10^{-5} m s^{-1}, and 2×10^{-5} m s^{-1}, respectively. K at each of these sites decreased by an order of magnitude over 150 days (Fig. 5E). In contrast, K at km 8.44 was initially steady at 10^{-5} m s^{-1} for 30 days, and then increased by a factor of 2–3 during the next 60 days.

An indication of across-channel and temporal variations in seepage rates and streambed properties is provided by records from three piezometers installed at km 11.42 (Fig. 6). There were significant differences in streambed seepage rates determined with these piezometers, with much more rapid seepage into the streambed on the right side of the channel, and slower seepage in the center and on the left side of the channel. Hydraulic gradients were similar at all three locations, and increased monotonically throughout the measurement period (Fig. 6C). Calculated hydraulic conductivities were generally greatest on the right side of the channel (where both the seepage rate and hydraulic gradient were greatest), and for much of the water year were an order of magnitude lower in the central and left side of the channel. The Pajaro River developed a dry gap at km 11.42 around day 308 of 2004, with essentially all discharge in the channel at km 0.00 lost to streambed seepage, although some small pools of stagnant water remained visible for the next several weeks. Discharge returned to km 11.42 on day 320 (because of an upstream dam release), and appears to have scoured fine-grained material out of the channel, temporarily increasing streambed K. Following this event, discharge continued to drop, more sediment was deposited on the bed (Fig. 4A), and K values continued to decrease as before (Fig. 6E).

4.4. Relations between streambed hydraulic conductivity, discharge, and seepage rate

A small fraction of the observed variations in streambed seepage rates along the experimental reach could have resulted from changes in fluid properties because of differences in temperature. The mean temperature in the stream channel over water year 2005 varied by 15 °C, equivalent to a change in fluid viscosity of ~30%. A 30% decrease in fluid viscosity would yield a commensurate increase in hydraulic conductivity rather than the characteristic decrease in conductivity observed later in the water year, when temperatures tend to be warmer. In addition, stream water tends to become warmer with distance downstream along the experimental reach, contrary to the overall decrease in streambed conductivity that occurs along the same interval.

Cross plots of streambed hydraulic conductivity, discharge, and seepage rate demonstrate several notable trends (Fig. 7). Hydraulic conductivity tended to decrease at lower discharge at km 8.13, km 9.84, and km 11.42, whereas conductivity tended to increase at lower discharge at km 8.44. The most likely explanation for the former trend is that fine-grained sediment was deposited in many locations at the lower end of the experimental reach when discharge decreased. The increase in conductivity at lower flows at km 8.44 may be related to the local geomorphology of the pool-riffle sequence at which this data was collected. Fine-grained sediment may collect in the pool near the top of this sequence, allowing water that continues to flow across the riffle to erode fine-grained material that was deposited earlier in the year. In addition, this is a location where seepage flows mainly upward from the streambed into the channel (Fig. 5C), which may help to reduce the deposition of fine-grained sediments as stream velocities are reduced (Rosenberry and Pitlick, 2009a,b).

A cross plot of streambed conductivity versus seepage rate suggests considerable hysteresis in the relation between these parameters (Fig. 7B). Conductivity decreased initially at km 8.13, km 9.84, and km 11.42 with more rapid seepage rates into the streambed, and conductivity continued to drop as seepage rates decreased later in the year. The latter trend is consistent with the clogging of the streambed by finer grained sediments, but the former trend may result because an increase in the negative head gradient

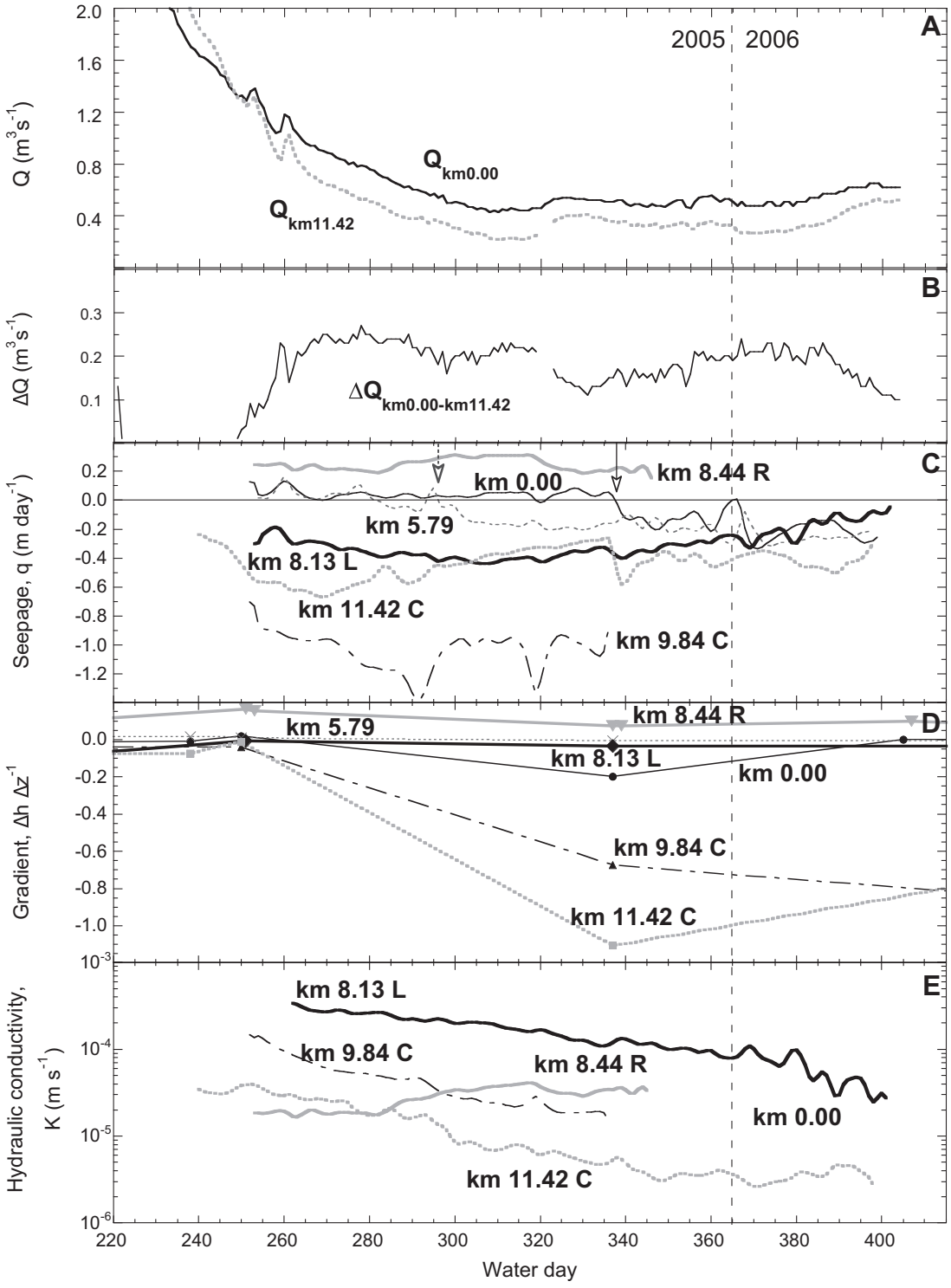

Fig. 5. Time series of stream and streambed processes and properties along the experimental reach of the Pajaro River in water year 2005 and the start of water year 2006 (May 8–November 20, 2005). (A) Daily mean discharge at the top, $Q_{km\ 0.00}$, and bottom, $Q_{km\ 11.42}$, of the experimental reach. (B) Channel discharge loss, ΔQ. (C) Seepage rate, q, at km 0.00, 5.79, 8.13, 8.44, 9.84 and 11.42. Arrows indicate water day when a location transitions from gaining to losing: (km 5.79 at water day 296 and km 0.00 at water day 338). (D) Measured and interpolated values of hydraulic gradient, and (E) hydraulic conductivity, K.

was able to overcome the decrease in conductivity caused by sediment deposition for a short time. The exception to this general trend is km 8.44, once again. At this site, conductivity increased along with the rate of upward seepage into the channel, but eventually both the seepage rate and the conductivity decreased once again late in the water year (Fig. 7B).

5. Discussion: implications of spatially and temporally varying seepage rates and hydraulic properties

Streambed hydraulic conductivity tended to decrease with distance along the lower half of the experimental reach of the Pajaro River, and the conductivity at individual sites that lose water into

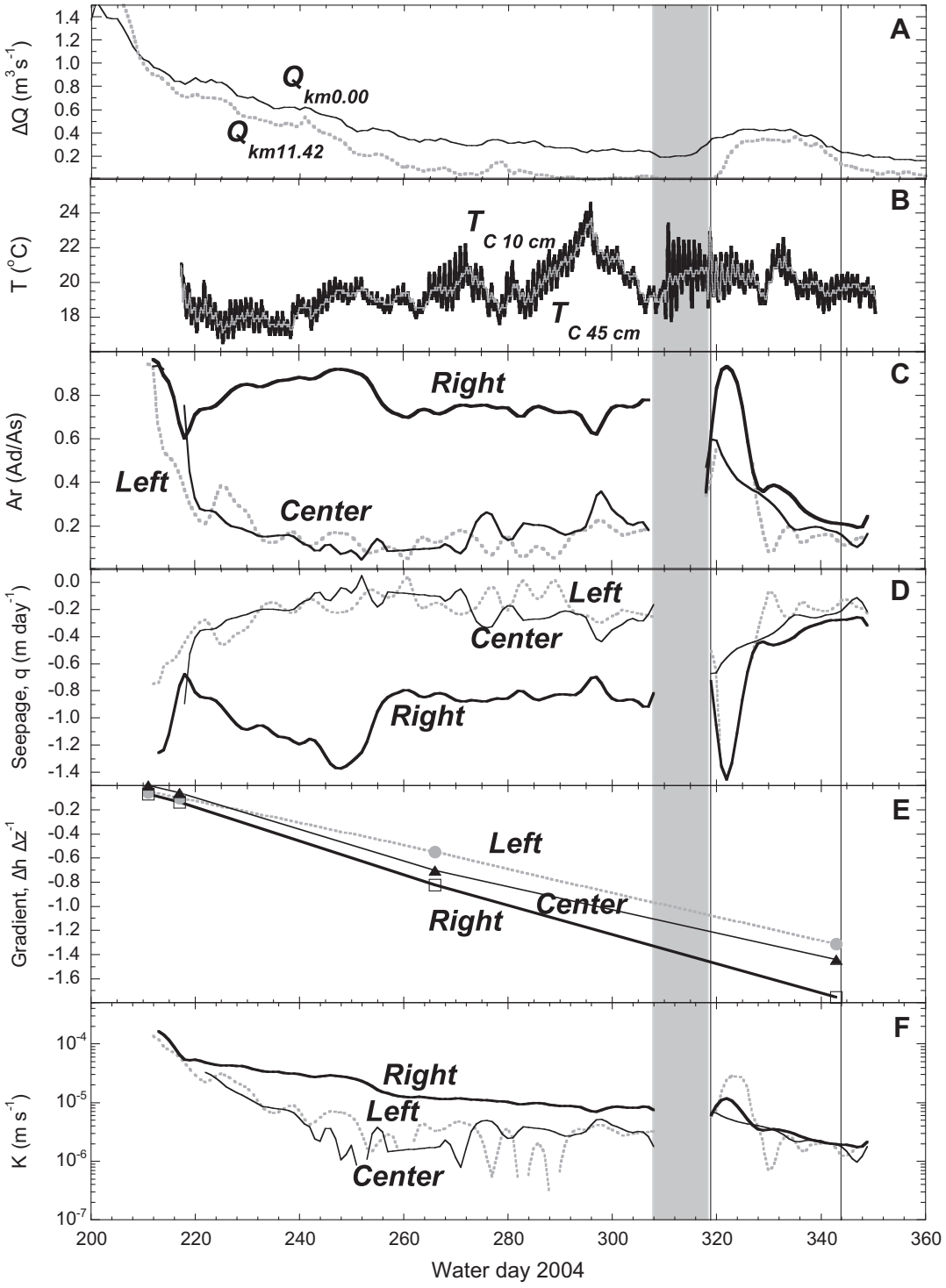

Fig. 6. Detailed hydrologic data from Pajaro River streambed piezometers *Left*, *Center*, and *Right* (looking upstream) at km 11.42 in water year 2004 (April 17–September 30, 2004). (A) Daily mean discharge at the top, $Q_{0.00}$, and bottom, $Q_{11.42}$, of the experimental reach. (B) Temperature measured at 15-min intervals at 10-cm and 45-cm depths below the base of the stream at *Center*. (C) Amplitude ratio, $Ar = A_{deep}/A_{shallow}$, between 10-cm and 45-cm thermographs at *Left*, *Center* and *Right*. (D) Seepage rate, q, (m day^{-1}), (E) Hydraulic gradient. (F) Hydraulic conductivity, K. Shaded area indicates a period (water day 308–318) when there was a dry gap and no channel discharge at km 11.42. An upstream dam release restored flow to the channel after this time.

the stream channel tended to decrease with time as discharge in the channel decreased. The combination of streambed geometry and high sediment load led to the spatial and temporal trends observed in streambed hydraulic properties. Sediment transport in the channel is reduced as discharge decreased late in the water year, particularly in the lower half of the experimental reach. This observation is consistent with the large-scale geomorphology of the channel, which is narrow and steep-sided where it passes through elevated areas along the upper part of the reach, and then widens with increasing distance downstream. The narrow and restricted nature of the upstream part of the channel results in a larger channel gradient and larger streamflow velocities, which minimize deposition of fine-grained sediment on the bed, even during relatively low-flows, whereas much more sediment is

Table 1
Summary of Pajaro River hydraulic data in water year 2004[a].

River km[b]	Seepage rate (m day^{-1})	Range	Hydraulic gradient (–)	Range	Hydraulic conductivity (m s^{-1})	Range[c]
0.00	0.09 ± 0.07	−0.03 to 0.31	−0.06 ± 0.03	−0.09 to −0.01		
5.79	−0.25 ± 0.10	−0.39 to −0.02	0.00 ± 0.00	−0.01 to 0.00	3.1×10^{-4}	
7.67	−0.21 ± 0.13	−0.45 to −0.08	−0.33 ± 0.09	−0.40 to −0.05	1.2×10^{-5}	1.6×10^{-6} to 7.6×10^{-5}
8.20	−0.53 ± 0.21	−0.99 to −0.17	−0.29 ± 0.13	−0.73 to −0.11	3.2×10^{-5}	6.2×10^{-6} to 1.3×10^{-4}
8.44[d]	−0.14 ± 0.27	−0.83 to 0.58	−0.02 ± 0.07	−0.40 to 0.31	4.7×10^{-5}	8.7×10^{-6} to 2.4×10^{-4}
9.84	−1.36 ± 0.64	−2.96 to −0.26	−0.78 ± 0.44	−1.38 to −0.15	1.1×10^{-4}	2.7×10^{-6} to 3.3×10^{-4}
11.42	−0.43 ± 0.42	−2.59 to −0.02	−0.97 ± 0.35	−1.71 to −0.21	5.8×10^{-6}	6.8×10^{-7} to 3.0×10^{-5}

[a] From water days 240–365.
[b] Data from km 7.67 is averaged for both, and data from km 8.44, 9.84 and 11.42 is averaged for all three piezometers at each location.
[c] No range provided for km 0.00 and km 5.79. Low hydraulic gradients yield large errors in hydraulic conductivity estimates, so K was not calculated for values smaller than the calculated limits of seepage $|q| < 0.05$ m day^{-1} or hydraulic gradient $|dh\ dz^{-1}| < 0.011$.
[d] Piezometers at km 8.44 are located at the bottom of a riffle and do not indicate regional longitudinal trends.

Table 2
Summary of Pajaro River hydraulic data in water year 2005[a].

River km[b]	Seepage rate (m day^{-1})	Range	Hydraulic gradient (–)	Range	Hydraulic conductivity (m s^{-1})	Range[c]
0.00	−0.05 ± 0.12	−0.34 to 0.13	−0.09 ± 0.06	−0.20 to 0.02	3.6×10^{-5}	
5.79	−0.13 ± 0.12	−0.32 to 0.16	0.00 ± 0.01	−0.01 to 0.01		
8.13	−0.31 ± 0.09	−0.44 to −0.05	−0.04 ± 0.02	−0.07 to −0.01	1.1×10^{-4}	1.1×10^{-5} to 3.4×10^{-4}
8.20	−0.35 ± 0.21	−0.73 to −0.11	−0.02 ± 0.02	−0.05 to 0.0	1.9×10^{-4}	7.2×10^{-5} to 2.6×10^{-4}
8.44[d]	0.11 ± 0.11	−0.08 to 0.31	0.08 ± 0.03	0.04 to 0.16	2.0×10^{-5}	5.8×10^{-6} to 4.1×10^{-5}
9.84	−0.75 ± 0.27	−1.38 to −0.15	−0.44 ± 0.25	−0.86 to −0.04	4.6×10^{-5}	4.9×10^{-6} to 1.7×10^{-4}
11.42	−0.51 ± 0.26	−1.71 to −0.21	−0.94 ± 0.46	−1.49 to −0.01	1.6×10^{-5}	1.7×10^{-6} to 4.0×10^{-4}

[a] From water days 240–365.
[b] Data from km 8.13 is averaged for both piezometers, from km 9.84 and 11.42 is averaged for all three, and from km 8.44, for all four piezometers at each location.
[c] No range provided for km 0.00 and km 5.79. Low hydraulic gradients yield large errors in hydraulic conductivity estimates, so K was not calculated for values smaller than the calculated limits of seepage $|q| < 0.05$ m day^{-1} or hydraulic gradient $|dh\ dz^{-1}| < 0.011$.
[d] Piezometers at km 8.44 are located at the bottom of a riffle and do not indicate regional longitudinal trends.

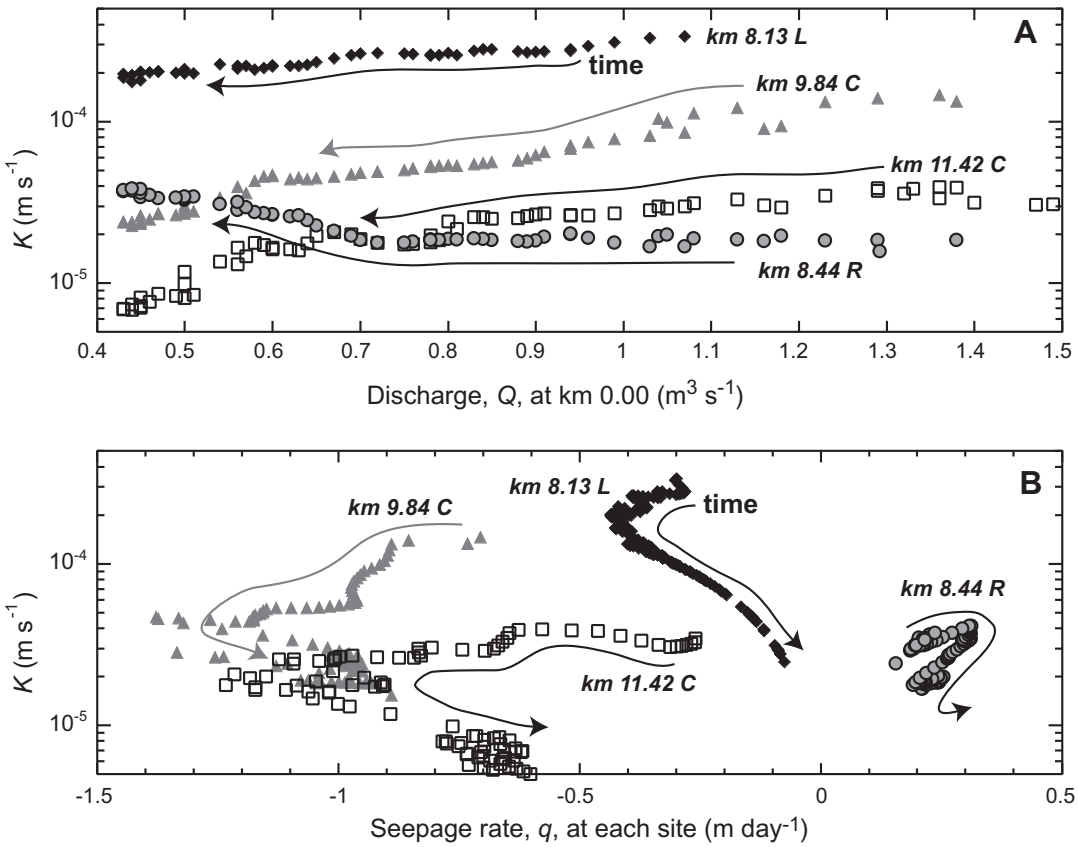

Fig. 7. Cross-plots of stream and streambed flows and properties along the Pajaro River experimental reach in water year 2005. (A) Hydraulic conductivity, K, versus daily mean discharge at the top of the experimental reach, $Q_{km\ 0.00}$ at km 8.13, 8.44, 9.84, and 11.42, and (B) K versus seepage rate, q, at each site. Arrows indicate progression with time. K decreases as $Q_{km\ 0.00}$ decreases at strongly losing locations km 8.13, 9.84 and 11.42, and K versus q values progress counter-clockwise, whereas K increases as $Q_{km\ 0.00}$ decreases at gaining location km 8.44, and K versus q values progress clockwise.

deposited downstream. The entire channel tends to be scoured out during high flows during the rainy season, and then the temporal pattern repeats as flows decrease during the second half of the water year. The decrease in K with time (through periods of low-flow) and subsequent streambed flushing during high flows are consistent with the clogging of the streambed by fine-grained sediments (e.g., Schalchli, 1992; Cunningham et al., 1987) or biofilms (Battin and Sengschmitt, 1999), both of which were observed in the Pajaro River.

This temporal pattern of changing flow, seepage, and streambed properties can also occur in association with smaller events, such as the short-term increase in channel discharge observed late in water year 2004 (Fig. 6). This increase in discharge briefly scoured the bed and increased the hydraulic conductivity and seepage rate, but as discharge decreased again, more sediment was deposited and both seepage and hydraulic conductivity decreased. Interestingly, the largest increase in seepage rate following this release occurred along the sides of the channel, rather than in the thalweg, as seen in models of a gaining stream (Storey et al., 2003).

Local-scale variations in streambed seepage are also generated by streambed topography (e.g., Storey et al., 2003; Kasahara and Wondzell, 2003) in a pool-riffle sequence. As expected, the Pajaro River generally loses discharge at the upstream end of pools (e.g., km 8.13), and gains at the downstream end of significant riffles (e.g., km 8.44). The dominantly upward flow at km 8.44 could reduce the deposition of fine-grained sediments as stream velocities are reduced, allowing K at this location to remain relatively constant, whereas decreases in K would prevail in dominantly losing stretches.

Changes in the relative connectedness between the stream and the underlying aquifer can also influence seepage patterns and apparent streambed conductivity values (e.g., Brunner et al., 2009b). As the ground water table becomes deeper beneath the stream later in the water year, losing reaches (e.g., sites at km 8.13, km 9.84, and km 11.42) may become more disconnected, while gaining reaches (such as km 8.44) remain connected. Where complete drying (2004 water days 308–320) and re-wetting of the channel at km 11.42 occurred (Fig. 6), changes in K and q through this period record the progression from connected to disconnected and back. It is possible that during the re-wetting period, hydraulic gradients were more variable than observed in this study (because gradient measurements were sparse), which would result in a less variable apparent K values.

Representing the processes and properties described in this study in models of surface water–ground water interaction would require taking into account numerous processes and relations that are not typically included in such models. For example, one could assign the streambed hydraulic conductivity to change according to a fixed schedule, but this would not be appropriate if the model included stream routing and discharge capabilities, so that flow in the channel varied with other processes being modeled. Instead, one could use observed, largely-monotonic relations between streambed hydraulic conductivity and channel discharge (Fig. 7A) to link these two terms. Streambed hydraulic conductivity could be calculated as a function of discharge, which itself would be determined (iteratively) by the model. In cases where channel discharge is large (greater than several $m^3\ s^{-1}$), the change in streambed conductivity would not greatly influence calculated discharge values. Within a model of the Pajaro River, the change in conductivity could change seepage loss such that the modeled stream would go dry or continue to flow, depending on actual parameter values used in the simulation. A more realistic (and challenging) model would include sediment load information, and account for changes to streambed thickness as discharge decreases and fine sediments are deposited. One might also attempt to include the hysteretic relation observed between streambed conductivity and seepage rate (Fig. 7B), but ideally this relation would come out of model predictions rather than being predetermined.

6. Conclusions

Seepage losses from 11.42 km-long experimental reach of the Pajaro River during the second half of water years 2003–2006 were generally 0.1–0.3 $m^3\ s^{-1}$. Much of this loss occurred within the lower part of the reach, consistent with the geology and hydrogeology below the stream channel. There were significant changes in stream channel morphology observed along the experimental reach, with the greatest changes noted in the lower half of the reach, where thick accumulations of fine-grained sediment were deposited as channel discharge decreased at the end of each water year.

Point seepage rates were determined along the experimental reach using time-series thermal methods. Seepage was downward into the streambed along most of the reach, at rates as great at $-1.4\ m\ day^{-1}$, except within a pool-riffle sequence where there was generally upward seepage into the channel. Streambed seepage rates were combined with hydraulic gradient data to determine spatially and temporally varying values of effective streambed hydraulic conductivity. Streambed hydraulic conductivity varied spatially between 10^{-6} and $10^{-4}\ m\ s^{-1}$, and tended to decrease (by an order of magnitude or more) as discharge in the channel decreased during the last half of the water year. One exception to this trend was within a pool-riffle sequence where there was upward seepage, which may have helped to minimize the deposition of fine-grained sediments during periods of low discharge.

This study elucidates quantitative relations between stream discharge, streambed seepage, and the hydraulic conductivity of the streambed. Our results suggest that efforts to control excess sediment load in streams can contribute to more vigorous surface water–ground water interactions. Controlling sediment load may enhance ground water recharge through streams, which can be critical in settings like the Pajaro Valley where limited groundwater resources are increasingly in demand. Controlling the sediment load in streams can also help to increase the rate of nutrient cycling through hyporheic exchange (e.g., Grimm and Fisher, 1984; Bencala, 1993; Dahm et al., 1998; Ruehl et al., 2007 and other studies), assist with flood control, and provide additional riparian benefits.

Clearly streambed hydraulic conductivity can be dynamic and highly variable. More work is needed both to assess spatial and temporal variations in streambed seepage and hydraulic conductivity with time, across a variety of natural systems, and to develop approaches that will allow representation of this dynamic behavior in computer models of surface water–ground water interactions.

Acknowledgements

This work was funded by the US Department of Agriculture (projects 2003-35102-13531 and 2002-34424-11762), the UCSC Committee on Research, and the UCSC Center for Agroecology and Sustainable Food Systems, and National Institutes for Water Resources 2007CA195G. Partial support for this work was provided by the U.S. Bureau of Reclamation agreement 06FC204044. We gratefully acknowledge Jonathan Lear and colleagues with the Pajaro Valley Water Management Agency for assistance with site access, data collection, and field support. In addition, the authors gratefully acknowledge field assistance provided by Gerhardt Epke, Remy Nelson, Emily Underwood, Laura Roll, Randy Goetz, Andy Shriver, Bowen Jenkins-Warrick, Robert Sigler, and Iris DeSerio. Dave Prudic provided a preprint review that significantly improved

this manuscript. We appreciate Don Rosenberry and Philip Brunner for their insightful reviews of this work.

Appendix A. Supplementary material

Supplementary data associated with this article can be found, in the online version, at doi:10.1016/j.jhydrol.2010.05.046.

References

Allen, D.M., Mackie, D.C., Wei, M., 2004. Groundwater and climate change: a sensitivity analysis for the Grand Forks aquifer, southern British Columbia, Canada. Hydrogeology Journal 12 (3), 270–290.

Barlow, J.R.B., Coupe, R.H., 2009. Use of heat to estimate streambed fluxes during extreme hydrologic events. Water Resources Research 45 (1), W01403. doi:10.1029/2007WR006121.

Battin, T.J., Sengschmitt, D., 1999. Linking sediment biofilms, hydrodynamics, and river bed clogging: evidence from a large river. Microbial Ecology 37 (3), 185–196.

Becker, M.W., Georgian, T., Ambrose, H., Siniscalchi, J., Fredrick, K., 2004. Estimating flow and flux of ground water discharge using water temperature and velocity. Journal of Hydrology 296 (1–4), 221–233.

Bencala, K.E., 1993. A perspective on stream-catchment connections. Journal of the North American Benthological Society 12 (1), 44–47.

Bower, D., Hannah, D.M., McGregor, G.R., 2004. Techniques for assessing the climatic sensitivity of river flow regimes. Hydrological Processes 18 (13), 2515–2543.

Brunner, P., Cook, P.G., Simmons, C.T., 2009a. Hydrogeologic controls on disconnection between surface water and groundwater. Water Resources Research 45, W01422. doi:10.1029/2008WR006953.

Brunner, P., Simmons, C.T., Cook, P.G., 2009b. Spatial and temporal aspects of the transition from connection to disconnection between rivers, lakes and groundwater. Journal of Hydrology 376 (1–2), 159–169. doi:10.1016/j.hydrol.2009.07.023.

Buchanan, T.J., Somers, W.P., 1969. Discharge Measurements at Gaging Stations, Techniques of Water-resources Investigations of the United States Geological Survey. Book 3: Applications of Hydraulics. US Government Printing Office, Washington, DC, pp. 1–65.

California State of Regional Water Quality Control Board – Central Coast Region, 2005. Final Project Report: Pajaro River Total Maximum Daily Loads for Sediment (including Llagas Creek, Rider Creek, and San Benito River), Regional Water Quality Control Board, San Luis Obispo, CA.

CARA, 1997. In: California Rivers Assessment Interactive Web Database University of California, Davis, CA.

Cardenas, M.B., 2010. The thermal skin effect of pipes in streambeds and its implications on groundwater flux estimation using diurnal temperature signals. Water Resources Research 46 (3), W03536. doi:10.1029/2009WR008528.

Cunningham, A.B., Anderson, C.J., Bouwer, H., 1987. Effects of sediment-laden flow on channel bed clogging. Journal of Irrigation and Drainage Engineering 113 (1), 106–118.

Dahm, Clifford N. et al., 1998. Nutrient dynamics at the interface between surface waters and groundwaters. Freshwater Biology 40, 427–451.

Dupré, W.R., Clifton, H.E., Hunter, R.E., 1980. Modern sedimentary facies of the open Pacific coast and Pleistocene analogs from Monterey Bay, California. In: Proceedings of the Quaternary Depositional Environments of the Pacific Coast. Pacific Section, Society of Economic Paleontologists and Mineralogists, Los Angeles, CA, United States (USA), Bakersfield, CA, United States, pp. 105–120.

EPA US, 2009. Detailed TMDL Report 32675: Pajaro River Sediment TMDL. In: USEP Agency, Total Maximum Daily Loads, US Environmental Protection Agency.

Fanelli, R.M., Lautz, L.K., 2008. Patterns of water, heat, and solute flux through streambeds around small dams. Ground Water 46 (5), 671–687.

Goderniaux, P. et al., 2009. Large scale surface–subsurface hydrological model to assess climate change impacts on groundwater reserves. Journal of Hydrology 373, 122–138.

Goto, S., Yamano, M., Kinoshita, M., 2005. Thermal response of sediment with vertical fluid flow to periodic temperature variation at the surface. Journal of Geophysical Research-Solid Earth 110 (B1).

Grimm, N.B., Fisher, S.G., 1984. Exchange between Interstitial and Surface Water: Implications for Stream Metabolism and Nutrient Cycling. HB 111, pp. 219–228.

Groves, D.G., Yates, D., Tebaldi, C., 2008. Developing and applying uncertain global climate change projections for regional water management planning. Water Resources Research 44, W12413. doi:10.1029/2008WR006964.

Haggerty, R., Argerich, A., Marti, E., 2008. Development of a "smart" tracer for the assessment of microbiological activity and sediment–water interaction in natural waters: the resazurin–resorufin system. Water Resources Research 44, W00D01. doi:10.1029/2007WR006670.

Hanson, R.T., 2003. Geohydrologic Framework of Recharge and Seawater Intrusion in the Pajaro Valley, Santa Cruz and Monterey Counties, California. 03-4096, US Geological Survey, Sacramento, CA.

Hanson, R.T., Dettinger, M.D., 2005. Ground water/surface water responses to global climate simulations, Santa Clara-Calleguas Basin, Ventura, California. Journal of the American Water Resources Association, 517–536.

Hatch, C.E., Fisher, A.T., Revenaugh, J.S., Constantz, J., Ruehl, C., 2006. Quantifying surface water–groundwater interactions using time series analysis of streambed thermal records: method development. Water Resources Research 42 (10), W10410. doi:10.1029/2005WR004787.

Healy, R.W., 2008. Simulating water, solute, and heat transport in the subsurface with the VS2DI software package. Vadose Zone Journal 7 (2), 632–639.

Healy, R.W., Ronan, A.D., 1996. Documentation of Computer Program VS2DH for Simulation of Energy Transport in Variably Saturated Porous Media; Modification of the US Geological Survey's Computer Program VS2DT, WRI 96-4230.

Jefferson, A., Nolin, A., Lewis, S., Tague, C., 2008. Hydrogeologic controls on streamflow sensitivity to climate variation. Hydrological Processes 22 (22), 4371–4385.

Johnson, M.J., Londquist, C.J., Laudon, J., Mitten, H.T., 1988. Geohydrology and Mathematical Simulation of the Pajaro Valley Aquifer System, Santa Cruz and Monterey counties, California. WRI 87-4281, US Geological Survey, Reston, VA.

Kalbus, E., Reinstorf, F., Schirmer, M., 2006. Measuring methods for groundwater–surface water interactions: a review. Hydrology and Earth System Sciences 10 (6), 873–887.

Kasahara, T., Wondzell, S.M., 2003. Geomorphic controls on hyporheic exchange flow in mountain streams. Water Resource Research 39 (1), 1005. doi:10.1029/2002WR001386.

Kipp, K.L., 1987. HST3D: A Computer Code for the Simulation of Heat and Solute Transport in Three-dimensional Ground-water Flow Systems. WRI 86-4095, US Geological Survey.

Kipp, K.L., 1997. Guide to the Revised Heat and Solute Transport Simulator: HST3D – Version 2. WRI 97-4157, US Geological Survey.

Lautz, 2010. Impacts of non-ideal field conditions on vertical water velocity estimates from streambed temperature time series. Water Resources Research 46 (1), W01509. doi:10.1029/2009WR007917.

Lee, D.R., Cherry, J.A., 1978. A field exercise on groundwater flow using seepage meters and mini-piezometers. Journal of Geological Education 27 (1), 6–10.

Lettenmaier, D.P., Wood, A.W., Palmer, R.N., Wood, E.F., Stakhiv, E.Z., 1999. Water resources implications of global warming: a US regional perspective. Climatic Change 43, 537–579.

Loheide, S.P. et al., 2009. A framework for understanding the hydroecology of impacted wet meadows in the Sierra Nevada and Cascade Ranges, California, USA. Hydrogeology Journal 17 (1), 229–246.

McDonald, M.G., Harbaugh, A.W., 1988. A Modular Three-dimensional Finite-difference Ground-water Flow Model US Geological Survey, Cheyenne, Wyoming.

Metzger, L.F., 2002. Streamflow Gains and Losses Along San Francisquito Creek and Characterization of Surface-water and Ground-water Quality, southern San Mateo and Northern Santa Clara Counties, California, 1996–1997. WRI 02-4078, US Geological Survey.

Muir, K.S., 1972. Geology and Ground water of the Pajaro Valley area, Santa Cruz and Monterey Counties, California. 4022-02, USGS Water Resources Division, Menlo Park, CA.

Murdoch, L.C., Kelly, S.E., 2003. Factors affecting the performance of conventional seepage meters. Water Resources Research 39 (6), 1163. doi:10.1029/2002WR001347.

Prudic, D.E., Konikow, L.F., Banta, E.R., 2004. A new streamflow-routing (SFR1) Package to Simulate Stream–Aquifer Interaction with MODFLOW-2000, OF 2004-1042, US Geological Survey, Reston.

Pruess, K., 1994. TOUGH2; transport of unsaturated groundwater and heat simulator. Bulletin – Geothermal Resources Council 23 (4), 142–143.

Pruess, K., Oldenburg, C.M., Moridis, G.J., 1998. Overview of TOUGH2, version 2.0. In: Pruess, K. (Ed.), LBNL – Lawrence Berkeley National Laboratory, Report: LBNL-41995, University of California, Lawrence Berkeley National Laboratory, pp. 307–314.

Puckett, L.J. et al., 2008. Transport and fate of nitrate at the ground-water/surface-water interface. Journal of Environment Quality 37, 1034–1050. doi:10.2134/jeq2006.0550.

PVWMA, 1999. Pajaro Valley Water Management Agency Local Water Supply Project, Pajaro Valley Water Management Agency, Watsonville, CA.

PVWMA, 2001. Pajaro Valley Water Management Agency State of the Basin Report, Pajaro Valley Water Management Agency, Watsonville, CA.

Rantz, S.E., 1982. Measurement and Computation of Streamflow, 2175. US Geological Survey, Washington, DC.

Rose, C., Adams, M., 2009. California, State of, Regional Water Quality Control Board – Central Coast Region Central Coast Ambient Monitoring Program (CCAMP), Pajaro River Data. Regional Water Quality Control Board, San Luis Obispo, CA (Personal Communication).

Rosenberry, D.O., 2008. A seepage meter designed for use in flowing water. Journal of Hydrology 359 (1–2), 118–130.

Rosenberry, D.O., LaBaugh, J.W., 2008, Field Techniques for Estimating Water Fluxes Between Surface Water and Ground Water. US Geological Survey Techniques and Methods, 128 p (Chapter 4-D2).

Rosenberry, D.O., Pitlick, J., 2009a. Effects of sediment transport and seepage direction on hydraulic properties at the sediment–water interface of hyporheic settings. Journal of Hydrology 373 (3–4), 377–391.

Rosenberry, D.O., Pitlick, J., 2009b. Local-scale spatial and temporal variability of seepage in a shallow gravel-bed river. Hydrological Processes 23, 3306–3318.

Ruehl, C. et al., 2006. Differential gauging and tracer tests resolve seepage fluxes in a strongly-losing stream. Journal of Hydrology 330 (1–2), 235–248.

Ruehl, C. et al., 2007. Nitrate dynamics within the Pajaro River, a nutrient-rich, losing stream. Journal of the North American Benthological Society 26 (2), 191–206.

Runkel, R.L., 1998. One-dimensional Transport with Inflow and Storage (OTIS): A Solute Transport Model from Streams and Rivers, US Geological Survey, Denver, CO.

Runkel, R.L., 2000. Using OTIS to Model Solute Transport in Streams and Rivers. FS-138-99, USGS, Denver, CO.

Sanford, W., 2002. Recharge and groundwater models: an overview. Hydrogeology Journal 10 (1), 110–120.

Sauer, V.B., Meyer, R.W., 1992. Determination of Error in Individual Discharge Measurements, OF 92-0144, US Geological Survey.

Schalchli, U., 1992. The clogging of coarse gravel river beds by fine sediment. Hydrobiologia (235/236), 189–197.

Schmidt, C., Conant, B., Bayer-Raich, M., Schirmer, M., 2007. Evaluation and field-scale application of an analytical method to quantify groundwater discharge using mapped streambed temperatures. Journal of Hydrology 347 (3–4), 292–307.

Smith, J.W.N., Bonell, M., Gibert, J., McDowell, W.H., Sudicky, E.A., Turner, J.V., Harris, R.C., 2008. Groundwater–surface water interactions, nutrient fluxes and ecological response in river corridors: translating science into effective environmental management. Hydrological Processes 22 (1), 151–157.

Snyder, M.A., Bell, J.A., Sloan, L.C., Duffy, P.B., Govindsamy, B., 2002. Climate responses to a doubling of atmospheric carbon dioxide for a climatically vulnerable region. Geophysical Research Letters 29 (11), 1514.

Stallman, R.W., 1965. Steady one-dimensional fluid flow in a semi-infinite porous medium with sinusoidal surface temperature. Journal of Geophysical Research-Solid Earth 70 (12), 2821–2827.

Stemler, G.F., 2005. Geologic Controls on Stream Seepage in the Pajaro Valley, Central Coastal California. Master of Science Thesis, University of California, Santa Cruz, Santa Cruz, CA, 51 pp.

Storey, R.G., Howard, K.W.F., Williams, D.D., 2003. Factors controlling riffle-scale hyporheic exchange flows and their seasonal changes in a gaining stream: A three-dimensional groundwater flow model. Water Resources Research 39 (2). doi:10.1029/2002WR001367.

Taniguchi, M., Burnett, W.C., Ness, G.D., 2008. Integrated research on subsurface environments in Asian urban areas. Science of the Total Environment 404, 377–392.

Therrien, R., McLaren, R.G., Sudicky, E.A., Panday, S.M., 2006, HydroGeoSphere: A Three-dimensional Numerical Model Describing Fully-integrated Subsurface and Surface Flow and Solute Transport, Groundwater Simulations Group, University of Waterloo, Waterloo, Canada, 378 pp.

Whiting, P.J., 2002. Streamflow necessary for environmental maintenance. Annual Reviews of Earth and Planetary Science 30, 181–206.

Wondzell, S.M., LaNier, J., Haggerty, R., 2009. Evaluation of alternative groundwater flow models for simulating hyporheic exchange in a small mountain stream. Journal of Hydrology 364 (1–2), 142–151.